Geophysical Research Letters

RESEARCH LETTER
10.1029/2020GL091187

Special Section:
China-France Oceanography Satellite(CFOSAT): Scientific Applications

New Directional Wave Satellite Observations: Towards Improved Wave Forecasts and Climate Description in Southern Ocean

L. Aouf[1,†], D. Hauser[2], B. Chapron[3], A. Toffoli[4], C. Tourain[5], and C. Peureux[6]

[1]DirOP-CNRM, Toulouse, France, [2]LATMOS/IPSL, Guyancourt, France, [3]IFREMER, Brest, France, [4]The University of Melbourne, Melbourne, Australia, [5]CNES, Toulouse, France, [6]CLS, Brest, France

†Current address: Météo-France, DirOP/MAR, 42 Avenue Gaspard Coriolis, Toulouse 31057 Cedex 1, France.

Abstract In spite of continuous improvements of ocean wave models in the last decades, large errors still remain in particular under strongly forced conditions, often encountered in the Southern Ocean, where strong westerly winds generate some of the fiercest waves on Earth in almost unlimited fetch conditions. The newly launched China-France Oceanography SATellite (CFOSAT) provides directional spectra of ocean waves for both wind seas and swells. Compared to Synthetic Aperture Radar (SAR), it can resolve shorter wavelengths in all directions, which dominate in non-fully developed wind waves. Here, the assimilation of these CFOSAT wavenumber components is proved to bring more accurate predictions of wave growth compared to the assimilation of significant wave height alone. A notable reduction of model bias is found in the Southern Ocean, especially in the Pacific Ocean sector. Results further exhibit a downward shift of the wave age, consistent with theoretical wave growth curves.

Plain Language Summary This work focuses on the importance of using directional wave observations to improve model wave prediction in the Southern Ocean. The results indicate a significant impact on the transition from a wind-dependent sea to a well-developed sea. A direct consequence of this work will concern a better understanding of the wave climate in the Southern Ocean and therefore, an improvement of coupled ocean/waves/atmosphere systems.

Key Points:

- The assimilation of directional wavenumber components in the wave model MFWAM induces a significant reduction of Significant Wave Height (SWH) bias in the Southern Ocean
- Data assimilation reveals the improvement of the energy transfer of wind waves during the wave growth phase under unlimited fetch conditions in the Pacific sector of the Southern Ocean
- The wave age and dominant wavenumber can significantly be corrected by assimilating directional observations of Surface Wave Investigation Measurements, compared with assimilation of SWH-nadir only

Correspondence to:
L. Aouf,
lotfi.aouf@meteo.fr

Citation:
Aouf, L., Hauser, D., Chapron, B., Toffoli, A., Tourain, C., & Peureux, C. (2021). New directional wave satellite observations: Towards improved wave forecasts and climate description in Southern Ocean. *Geophysical Research Letters*, *48*, e2020GL091187. https://doi.org/10.1029/2020GL091187

Received 8 OCT 2020
Accepted 4 JAN 2021

1. Introduction

The accuracy of wave prediction models has increased notably over the past decade, following the improvement of atmospheric models, which provide the wind forcing. Furthermore, development of assimilation techniques has allowed the incorporation of satellite data into models to optimize performances (Lionello et al., 1992). In this respect, space-borne altimeter sensors provide global estimates of significant wave height—a measure of the overall energy content of the wavy surface—which contributes to adjusting the variance of the wave energy spectrum. Moreover, Synthetic Aperture Radar (SAR) technology provides high resolution surface observations that can be converted into directional wave energy spectra. Assimilation of the latter further enables a more comprehensive control of the energy density function, not only allowing the optimization of the variance, but also controlling wave periods and wave directions (Aouf et al., 2019). Nevertheless, SAR only robustly detects swell systems, that is, a long wave system no longer under the effect of local wind, with wavelength longer than 200 m (Collard et al., 2005). The wind sea part cannot always be resolved, when propagating near along the satellite direction (Chapron et al., 2001), limiting the assimilation effectiveness.

Generation and growth of wind sea depend on the fetch conditions (Donelan et al., 1985; Hasselman et al., 1973; Young, 1999), with (nonlinear) energy transfer across wave scales, until an equilibrium state (full development) is reached. More specifically, the transfer consists of an inverse cascade transferring energy from high to low frequencies, which downshifts the spectral peak, stretches the wavelengths and consequently accelerates the wave phase speed. Growth ultimately stops, and the wind sea becomes swell, when the ratio of the wave phase speed to the wind speed (i.e., wave age) is larger than about 1.2 (atmosphere cannot force waves that move faster than the wind, Phillips, 1977; Pierson & Moskowitz, 1964). Concomitantly, there is a direct cascade occurs to shift energy toward high frequencies, forcing energy to dissipate mostly by wave breaking and to counterbalance the wind input.

Energy further redistributes across directions so that, near the peak, the wave spectrum narrowed during growth (e.g., Donelan et al., 1985; Fadaeiazar et al., 2020; D. E. Hasselmann et al., 1980). The directional distribution and integrated values, such as the mean wave direction are crucial parameters affecting wave growth through wind input, as the atmosphere forces energy into wave components that are aligned (and almost aligned) with wind (Gunther et al., 1981). However, directional properties remain one of the less known properties of the ocean surface. Contemporary wave models heavily use parametrizations to shape the directional spreading during the wave growth, assuming the directional distribution being unimodal (i.e., energy is concentrated around one dominant direction, Donelan et al., 1985; D. E. Hasselmann et al., 1980; Mitsuyasu et al., 1975) and defined by a directional spreading function of the form $\cos^{2s}(\theta)$, where θ is the wave propagation direction. Today no general consensus has been reached on the exact shape of the directional distribution. Moreover, field and laboratory observations have also suggested that the nonlinear interactions can induce a bimodal directional distribution in the early state of wave growth (Ewans, 1998; Toffoli et al., 2010, 2017; Young et al., 1995), with the angle of separation among peaks depending on the wave age and wind direction (Long & Resio, 2007). Peaks eventually merge into a unimodal directional function consistent with $\cos^{2s}(\theta)$ when approaching full development (e.g., Fadaeiazar et al., 2020; Toffoli et al., 2017).

Such uncertainties on the directional properties affect the identification of those wave components that are aligned with the wind, and thus translate into errors in the estimation of the wind input process in the wave prediction model. The extent of these errors is yet to be quantified. As contemporary satellite products cannot fully optimize wind sea, the latter remains a notable source of model errors, resulting in an overestimation of significant wave height (positive bias). This is exacerbated in the Southern Ocean (Zieger et al., 2015)—a region covering an uninterrupted band of water around Antarctica south of the main landmasses of Africa, Australia, and South America—that is dominated by strong westerly winds, which blows all-the-year-round with almost unlimited fetches and speed in excess of 13 m/s during summer months and 18 m/s during winter months (Young et al., 2020). These intense winds generate some of the fiercest waves on the planet with high percentiles of wave height exceeding 5 m during summer and 7 m during winter (e.g., Babanin et al., 2019; Barbariol et al., 2019; Letraon et al., 2019; Vichi et al., 2019; Young et al., 2020).

The newly launched China-France Oceanography Satellite (CFOSAT) carries the Surface Wave Investigation Measurements (SWIM) sensor (Hasselmann et al., 2012)to help advance these studies. Compared to SAR estimates, SWIM can resolve directional properties for a broader range of wavelengths, from 70 to 500 m, to provide directional distribution of the wave energy that can include both wind sea and swell systems. Here, we discuss SWIM data assimilation on model performance in the Southern Ocean. We demonstrate that assimilating directional properties from SWIM improves prediction of energy transfer during wave growth and concurrently of significant wave height. We show that model bias is reduced more efficiently when compared with classical assimilation procedures that incorporate information on the significant wave height only.

2. CFOSAT Mission and SWIM Spectra

The instrument SWIM of CFOSAT is a real aperture scanning radar which provides directional wave spectra from several off-nadir beams (pointing at 6°, 8°, and 10°). Each spectrum is representative of an area of about ±35 km along-track by 90 km on each side of the nadir track, and is discretized over 32 wavenumbers from 0.0126 to 0.279 rad/m, corresponding to the wavelength domain 22–500 m, with a geometric progression of 1.1 and 12 directions, that is, every 15° with a 180° ambiguity in the propagation direction. During the calibration/validation phase of the mission a detailed analysis was carried out (see Hauser et al., 2020). Retrieval of the dominant direction, dominant wave height, and significant wave height was demonstrated and assessed. Except for waves propagating close to the along-track direction, two-dimensional wave spectra can be accurately recovered over the wavelengths range of 70–500 m (see Hauser et al., 2020). In this study, we used SWIM wave spectra derived from the most recent processing version V5.0 which has been shown to significantly reduce the noise impact on the detection of wave partitions (see Hauser et al., 2020); furthermore, we focus on the directional wave spectra from the beam 10°, demonstrated to perform the best. SWIM also provides Significant Wave Height (SWH) along its track from nadir measurements (every

~7 km), just like the classical altimeter measurement (referred to as SWIM-nadir). For the assimilation, we used observations made over a 36 days period from April 26 to June 1, 2019. During this period, 343,885 wave spectra from SWIM were collected for the global ocean, and 95,281 of which were from the Southern Ocean.

3. Numerical Model and Data Assimilation Technique

The MFWAM wave model describes the evolution of wave spectra in space and time through the wave action conservation equation with source terms representing the wave generation by the wind, the nonlinear interactions, and the wave breaking at sea surface. The wave model MFWAM of Meteo-France is based on the IFS-ECWAM computing code of the ECMWF (see IFS-38R2). The model MFWAM uses an ST4 dissipation term related to wave breaking proposed by Ardhuin et al. (2010). Also, in the MFWAM model, the wind input source term takes into account a dissipation term due to the damping of the swell by the surface friction. The nonlinear interactions are represented by the Discrete Interaction Approximation (DIA) which is a common approximation in numerical wave models due to its computational efficiency. The MFWAM model is used for the global wave system of the Copernicus Marine Service with a recent update which takes into account a spectra tail in the form of the Phillips' spectrum. This parameterization is important for the calculation of the total stress provided to the ocean model and the impact of waves on the atmosphere in a coupled simulation.

In the present study, the model MFWAM uses a discretization of the wave spectrum in 24 directions (from 0° to 360°) and 30 frequencies increasing from 0.035 Hz with a geometric progression of 1.1. The MFWAM model is set for a global configuration with a grid resolution of 0.5°. The model is forced by analyzed winds and sea-ice fraction provided by the IFS atmospheric system of the ECMWF. Four sets of simulations were run: (i) with assimilation of wavenumber components Kx and Ky from SWIM spectra (run A); (ii) with assimilation of SWIM SWH only (run B); (iii) with assimilation of both SWH and wavenumber components (run C); and (iv) without assimilation (run D) as a control run to examine the impact (or to build a benchmark database).

Wavenumber components were assimilated into the model with the following scheme (Aouf et al., 2006, 2019): (i) model and SWIM spectra are partitioned to separate wind sea from swell systems, following Gerling (1992); (ii) partitions of the model spectra are matched with the SWIM counterpart by minimizing their Cartesian distance between their mean wavenumbers. This cross-assignment process removes the SWIM partitions affected by the ambiguity of 180° and also avoids including corrupted partitions; (iii) an optimal interpolation between model and observations is applied to the two wavenumber components Kx and Ky of each partition mean wavenumber; and (iv) analyzed partitions are superposed to reconstruct the analyzed wave spectrum, with smoothing procedure to avoid gaps between partitions. Only modes with wavelengths greater than 70 m were used for the assimilation, while the first guess wave spectrum from the model stays unchanged otherwise.

The assimilation of SWH from SWIM instrument at nadir look consists in solely performing only the optimal interpolation scheme for SWH (as a stand-alone procedure or in conjunction with the assimilation of wavenumber components). Note, however, that assimilation of SWH further requires a scaling of the wave spectrum in the frequency range by using the empirical power laws developed in Lionello et al. (1992). This is the classical approach, used in most operational models (see Aouf & Lefèvre, 2015).

The study area focuses on the Southern Ocean where a large number of storm events with strong winds are generated during the Austral winter. We should remark that during the period of study, surface wind speeds exceeding 20 m/s represent 30% for the Pacific Southern Ocean between the longitudes 150°E−250°E.

The Southern Ocean is well covered by altimeter missions. Therefore, the validation of the model simulations is based on significant wave heights provided by the Jason-3, Saral/Altika, and Sentinel-3 altimetry missions in this region. Super-observations of SWH from altimeters have been generated on the grid size of the model, which is 0.5° × 0.5°, with about 665,249 collected points. Thus, to evaluate the impact of assimilation, we compare SWH from the four model runs with those provided by the altimeters on this grid size.

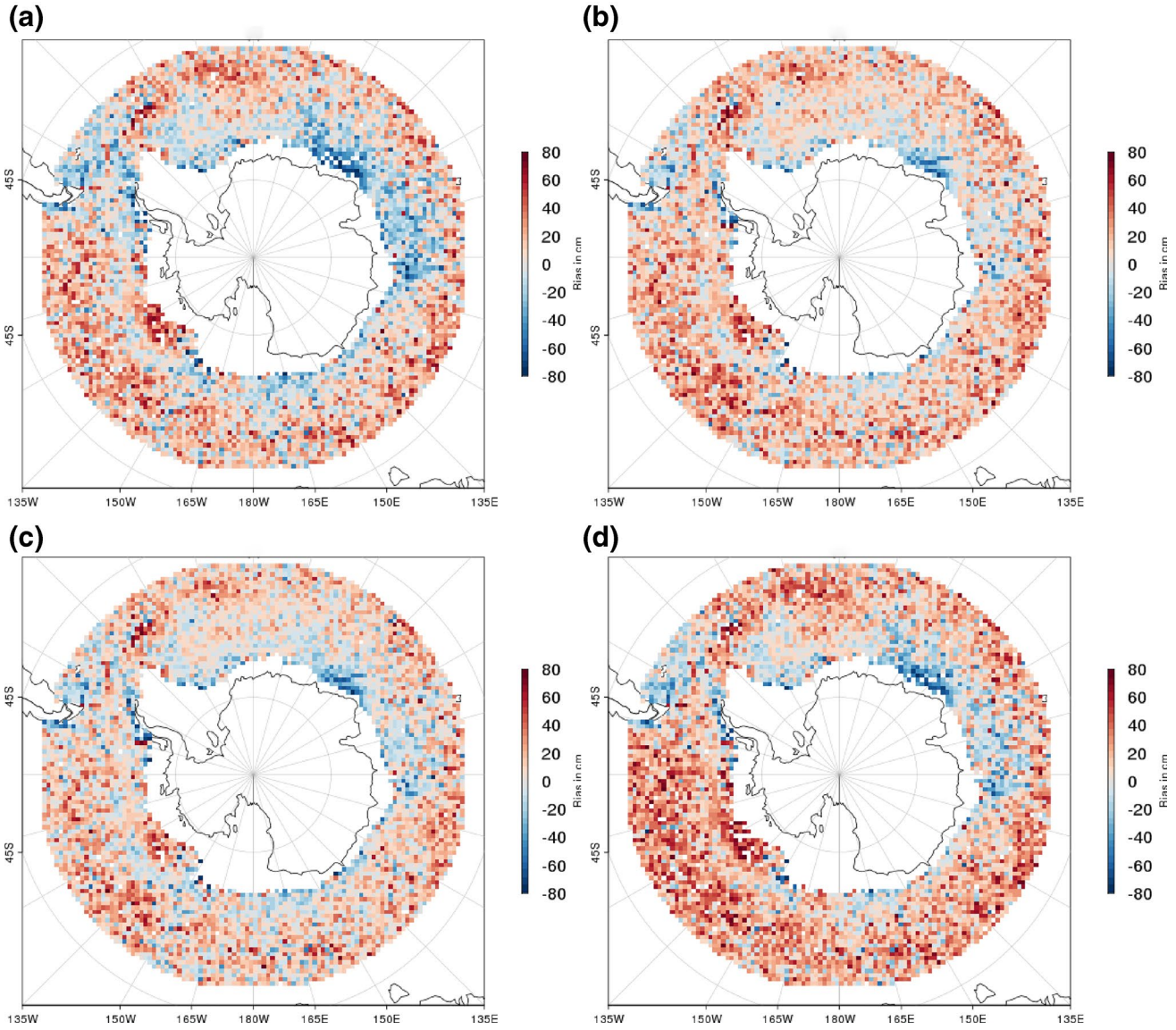

Figure 1. Bias maps of SWH (in cm) for simulations of the MFWAM model in comparison with altimeters Jason-3, Saral/Altika, and Sentinel-3 during the period starting from April 26 to June 1, 2019. (a), (b), (c) and (d) indicate runs A, B, C, and D, respectively. SWH, Significant Wave Height.

4. Results

Biases on SWH from the model runs, with respect to the independent altimeter data, are presented in Figure 1, maps covering the (50°S–70°S) area. For all runs, a dominant trend of positive bias can be identified in the Southern Ocean, with the highest values in the Pacific Southern Ocean. Negative biases of SWH are also observed in the Atlantic and Indian oceans near the Marginal Ice Zone (MIZ), where strong uncertainties are expected on local winds related to sea-ice melt-water. There is an evident bias reduction when satellite data are assimilated. On average, the control run (without assimilation) leads to a mean bias for SWH of approximately 0.13 m (Figure 1d) with maximum values reaching 1 m. The mean bias reduces to 0.10 m when assimilating satellite SWH estimates (Figure 1b). Incorporating wavenumbers in the assimilation further significantly contributes to reduce the bias, dropping to 0.03 m for assimilation of wavenumbers only (Figure 1a), and 0.05 m, when assimilating both wavenumbers and SWH (Figure 1c). The slight increase in bias in run C can be explained by the use of empirical power laws for wave growth (Lionello et al., 1992) to redistribute the corrections from assimilating SWH over the full wave spectrum. This reduces the benefit of directly correcting the partition (dominant wave train). In addition, the weight of the assimilation of SWH

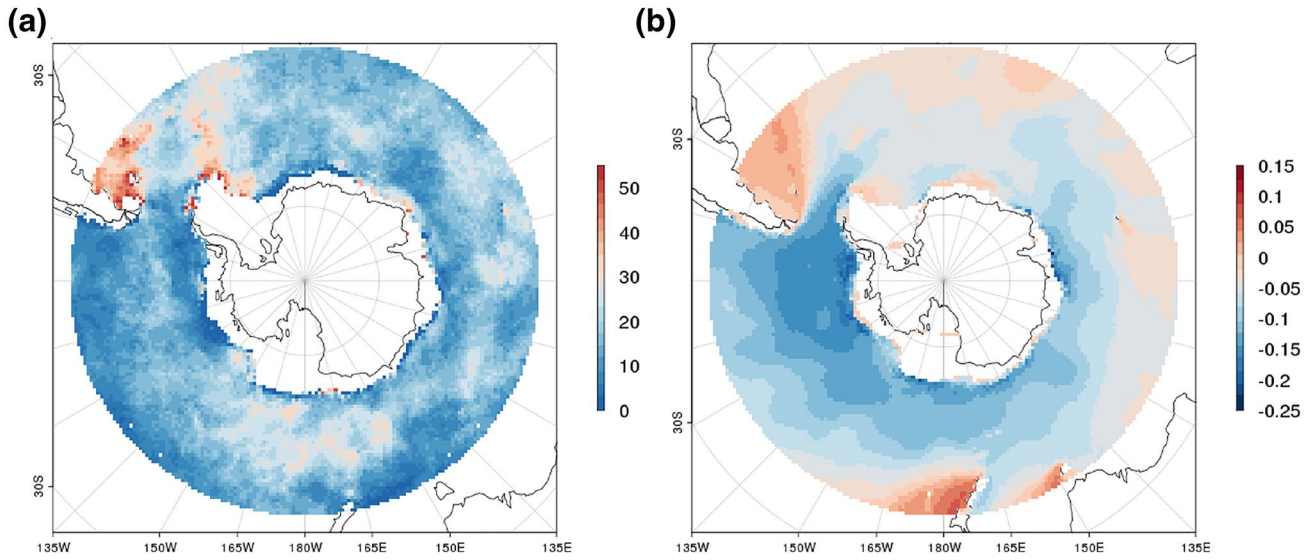

Figure 2. (a) Probability of occurrence (color code indicates percentage) of dominant wind sea state ($C_p/U_{10} < 1.2$) from model run (A) (b) Mean difference of SWH between run A and run D during the period from April 26 to June 1, 2019. SWH, Significant Wave Height.

in run C is greater because of the higher resolution of the observations (every ~7 km compared to 70 km for partitions).

To explore the impact of the assimilation on high waves generated by heavy storm conditions, a scatter analysis from MFWAM and altimeter sensors is performed for selected SWH larger than 5 m, which are mostly located in the Pacific sector (about 11,071 points). Overall, run A results in an excellent correlation with altimeter data, with scatter diagram following the slope 1:1 and intercept of 0.04 m, substantiating the significant bias reduction. On the contrary, run B shows an overestimation of model results, with data points distributed along a slope of 1.05, intercept of −0.19 m and a mean positive bias of 0.11 m. For run C, the slope and the intercept are 1.03 and −0.14, which show the improvement induced by the assimilation of wavenumbers compared to run (b) In terms of Normalized Root Mean Square Error (NRMSE), the best performance for large SWH (greater than 5 m), 10.3% is obtained when assimilating wavenumber components (runs A and C). For the assimilation of SWH only and the control run, NRMSE are about 10.6% and 11%, respectively.

To explain this result, it must be recalled that in the wind-wave growth phase, there is a transfer of wave energy from the high frequencies to the smaller frequencies, until an equilibrium state is reached. In general, the wind input term in a wave model which describes the wave growth depends, for each frequency, upon the difference between wave and wind directions. The fact that the assimilation of wavenumber components corrects both the wave direction and the dominant frequency directly leads to improved wave growth and the energy transfer for wind waves before the equilibrium state.

Also, recall that the wave age, expressed as the ratio of peak wave phase speed C_p and the surface wind speed U_{10}, indicates whether the sea state is wind sea or swell dominant. The wind sea can therefore be identified by a wave age C_p/U_{10} lower than 1.2. Figure 2a shows the regional distribution of wind sea, by the probability of occurrence associated with a wave age smaller than 1.2 (estimated over the analyzed period). In general, swell is dominant in the Southern Ocean; however, there are several regions where the occurrence of wind sea is important (30%–50%) like in the western sector of the Atlantic and Pacific ocean. This is due to the occurrence of relatively close storm systems, which limits fetches for wave growth.

Elsewhere, the low probability of wind sea (i.e., predominance of swell) indicates the presence of fully developed waves or swell, for instance in the Drake passage, Chile sector. Figure 2b shows the difference between the mean SWH derived from model runs with assimilation of partition wavenumber components (run A) and benchmark simulation (run D). The assimilation results in a significant reduction of the

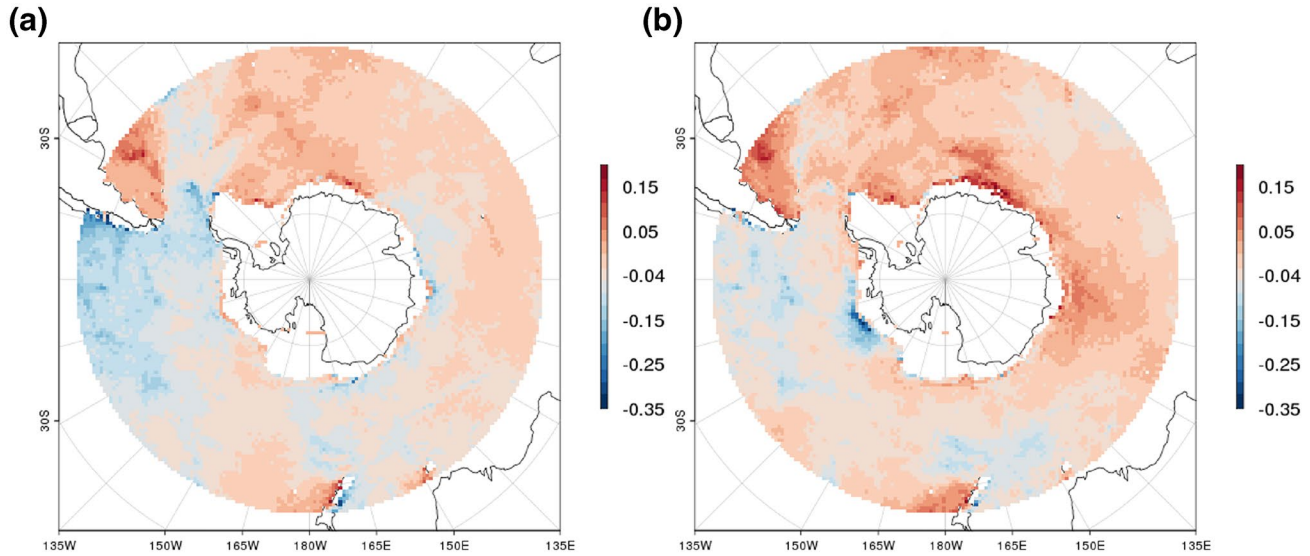

Figure 3. Average of difference of wave age (C_p/U_{10}) of runs with and without assimilation during the period between April 26 and June 1, 2019. (a) Stands for the assimilation of wavenumber components (run A), while (b) indicates the assimilation of SWH only. Negative values mean overestimation of wave age and conversely positive values indicate underestimation of the control run. SWH, Significant Wave Height.

significant wave height throughout the western part of the Southern Ocean in comparison with the control run. The extent of this difference depends on the wave age (cf. Figure 2a). Small differences are reported in the Atlantic Ocean and Indian Ocean Sector, where swell is not dominant (cf. Figure 2a), while the largest average differences—up to −0.25 m—are found in the Pacific Ocean sector, especially in the Amundsen Sea and Bellingshausen Sea subsectors and in the Drake passage. There are the areas where the wind sea generated South of New Zealand has transformed into a swell after a long, uninterrupted propagation.

Let us define the difference between assimilation runs and the control run the analysis increment. The impact of run A on the peak wave age indicates two trends on the analysis increment as shown in Figure 3a. The first trend concerns the Pacific Ocean sector and Drake Passage where there is a strong negative analysis increment on average which is linked to the overestimation of the wave age by the run D. The average difference in this sector reaches −0.25. The second trend is observed in the Atlantic and Indian oceans sectors, where we see that the assimilation of partitions wavenumbers induces a positive increment. This latter indicates an underestimation of the wave age by the control run D with a maximum average difference of 0.15. By comparing Figures 3a and 3b, we see that run B mainly indicates positive increments in all sectors and enhanced in some regions the impact in comparison with run A. The negative increment caused by run B is limited and not significant correction. This can be explained by the use of empirical power laws (Lionello et al., 1992) which seems less efficient to correct peak wave age in unlimited fetch conditions in Pacific sector of the Southern Ocean.

To investigate the difference between run A and run B, we analyzed the analysis increment of dominant wavenumbers from these two runs in comparison with the control run D Figures 4a and 4b show the analysis increment of the dominant wavenumber of runs A and B, respectively, as a function of SWH located on the altimeters tracks used for the bias evaluation in the Southern Ocean. Clearly, the assimilation of the partition wavenumbers mainly leads to a positive correction of the dominant wavenumber, k_p (Figure 4a), which indicates an underestimation of the control run D This increase of the wavenumber is most pronounced for high SWH (larger than 5 m), which shows that assimilation maintains the wave regime in the growth phase. Figure 4c reveals that the majority of the dominant wavenumbers k_p points are between the theoretical curves of young and mature seas as given by the Elfouhaily spectrum (ECMWF, 2013; Elfouhaily et al., 1997). Figure 4c further indicates a good consistency of the variation of dominant wavenumber with SWH in comparison with theoretical curves. On the contrary for run B (Figure 4b), we notice that the correction of k_p is dominated by negative analysis increments for strong SWH (larger than 5 m). This explains the difficulty of run B to reduce the bias for large SWH, and also to improve the dominant wavenumbers

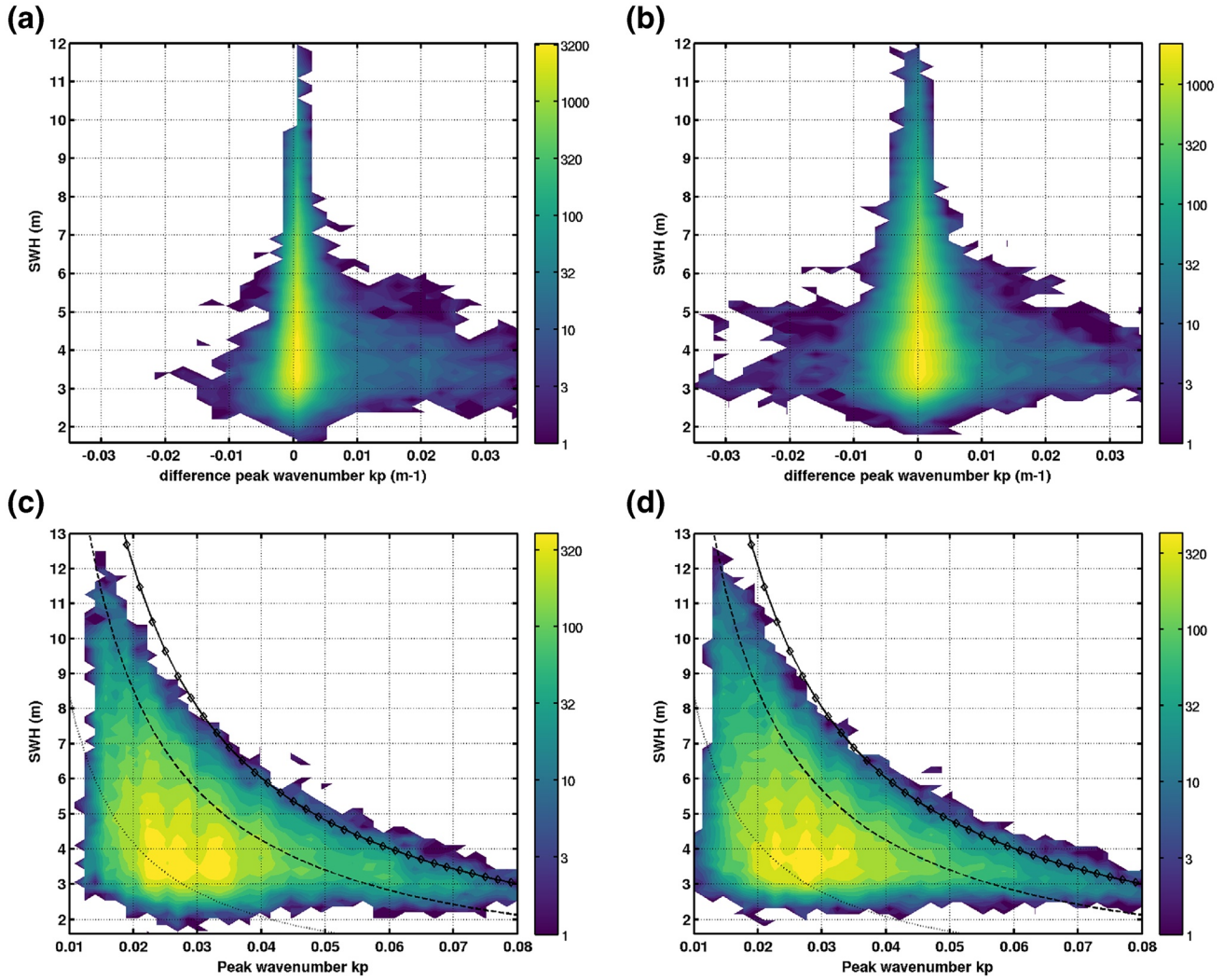

Figure 4. (a) and (b): variation of analysis increment of peak wavenumber with SWH, for model runs A and B, respectively. (c) and (d): relation between SWH peak wavenumber with, for model runs A and B, respectively. The dotted, dashed and diamond lines indicate the theoretical variation for peak wavenumber of young (wave age = 0.7), mature (wave age = 1), and fully developed (wave age = 1.2) seas according to the wave spectrum model of Elfouhaily et al. (1997). With Equations 37 and 38 in Elfouhaily et al. (1997), we obtained the following relation SWH = $(0.17/k_p)*\Omega^{-1.7}$ where Ω is the inverse wave age. Color bars indicate the density of points by pixel. SWH, Significant Wave Height.

during the growth phase. Figure 4d also indicates that the number of k_p points between the young and mature sea curves is smaller compared to Figure 4c.

5. Discussions

The peak group velocity (C_g) of waves for deep water depends on peak wavenumber, as $0.5*(g/k_p)^{0.5}$, where g is the gravity acceleration. The nonlinear interactions govern the peak frequency downshift as long as the waves are young. The process of wave growth in storm systems is then closely related to the fetch and wind duration conditions. Studies (e.g., Hsu et al., 2019; Kudryatsev et al., 2015) have evidenced the dependency between the wave group velocity (C_g) and storm displacement speed (V). For extra-tropical storms and based on self-similarity theory (Badulin et al., 2007), Kudryatsev et al. (2015) proposed a limiting condition of the wave group velocity, independent of wind speed, $C_{g\_max} = V/(1+q)$, where q depends on fetch laws. Considering JONSWAP growth conditions (Hasselman et al., 1976), $q = -3/10$, it leads to $C_{g\_max} = 10/7 * V$. Mature waves outrunning rapid extra-tropical storms are thus expected to reach large wavelengths and group velocities, independent of the maximum wind conditions. Today, this effect is not well taken into

account in numerical wave models and errors in the velocity of storm displacement may impact significantly the modeled wavefield. For severe storms the winds from atmospheric models are in general underestimated, and this is compensated by a larger wind action and slower velocity of storm displacement. In consequence, the wave model controlling the nonlinear interactions (fetch laws) with ad-hoc adjustments between wind-wave growth and wave breaking dissipation can partly reduce the misfit of the wind, but this is accompanied by enhance wave growth. This relation between C_g and V thus highlights the key advantage of assimilating observations of directional wavenumbers.

To explore the quantitative impact of the assimilation of wavenumbers on C_g in the Southern Ocean, we considered the points used in the validation with altimeters under wind sea wave regime (about 25,170 points corresponding to ~4% of the total). During the period of study, the mean and maximum C_g for run A are about 7.5 and 13.1 m/s, respectively, whereas they are 7.7 and 15.1 m/s, respectively, for run D. This indicates that in the mean, the assimilation of wavenumbers partitions reduced the overestimation of C_g by the model. By analyzing the distribution of the difference of C_g between runs A and D, the correction of underestimation of C_g concerns 26% of the points, while the correction of overestimation of C_g is about 64% of the points. Thus the assimilation wavenumbers helps control C_g directional properties during growth phase and evolution within and outside the large and rapid storms in the Southern Ocean, which favor trapping fetch conditions as described by Kudryatsev et al. (2015) or Hsu et al. (2019) for tropical or midlatitude storms. It is worth mentioning that corrections on C_g impact the wave steepness and related dissipation from wave breaking, which in turn modulates the upper ocean turbulence and mixing conditions. The decrease in C_g and related increase of wave steepness sustains the wind sea growth phase with enhanced nonlinear interactions.

In summary, the assimilation of wavenumbers partitions induces a significant reduction in SWH bias during the wave growth phase in the Southern Ocean. This is accompanied by a correction on the dominant wavenumber and wave age. The impact on group velocity indicates a change in the relative velocity between wave groups and storm displacement, which can result in an enhancement of the wave energy and wave breaking that affects the ocean mixing layer and air-sea interaction. The assimilation of wavenumber partitions shed lights on difficulties related to wind-wave generation in the wave model. This opens the development of better parametrizations to storm conditions in the Southern Ocean.

6. Conclusions

The Southern Ocean is dominated by strong wave systems which can strongly modulate air-sea interactions and ocean and sea-ice dynamics (e.g., Alberello et al., 2020; Hasselmann et al., 2012; Schamle et al., 2019; Thurnherr et al., 2020; Vichi et al., 2019). Contemporary wave models generally provide biased estimates of the significant wave height in this region, despite assimilation of satellite observations. However, assimilation methods are limited to significant wave height or truncated directional wave energy spectra, to mostly account for swell systems, but neglecting the short wave components of the wind sea. With the instrument SWIM carried by the CFOSAT satellite, it is now possible to more systematically detect directional wave propagation properties that resolve both swell and wind-wave systems. This study demonstrates that the assimilation of these directional wavenumber components from more comprehensive spectra enhances model prediction of energy transfer during the wave growth phase. This leads to improved estimation of the significant wave height in the Southern Ocean. The validation is conducted by comparing significant wave height from model runs with and without assimilation against observations from altimeter sensors. Overall, all data assimilation reduces biases. However, model runs with assimilation of wavenumber components (i.e., directional properties) are the most efficient with substantial bias reduction (from 13 cm bias without assimilation to 3 cm with assimilation) compared to assimilation of significant wave height only.

Results show that taking into account wavenumbers components can significantly correct the wave age and the dominant wavenumber in the Southern Ocean, to help control the transition between wind waves and mature sea regimes. This is verified with the theoretical growth curves (SWH as function with k_p). Overall, we observe a better spread of the impact on wave age when using directional observations around the Southern Ocean in comparison with the assimilation of significant wave height only. The transition to swell regime and the propagation in the Northern Ocean region is also well tracked as it is observed in

Pacific Ocean sector. Clearly, the assimilation of SWH only showed a limited and only localized impact on the wave age.

This research opens perspectives on the use of the directional capabilities of SWIM instrument on-board of the CFOSAT mission to improve wave model forecast. The assimilation of wavenumber components is promising and expected to improve the descriptions of ocean/atmosphere coupling in terms of both momentum and gas flux transfer in the Southern Ocean, which are still poorly understood in climate models.

Data Availability Statement

The level 2 data used here are processed by SWIM algorithms version V5.0.1. The quality controlled data are accessible on shared research depository zenodo following this URL web link: https://doi.org/10.5281/zenodo.4392511.

Acknowledgments
This work is funded by the French Space Agency CNES in the frame of TOSCA national program. The authors would also like to thank Alice Dalphinet and Malek Ghantous for helping with the preparation of the manuscript.

References

Alberello, A., Bennetts, L., Heil, P., Eayrs, C., Vichi, M., MacHutchon, K., et al. (2020). Drift of pancake ice floes in the winter Antarctic marginal ice zone during polar cyclones. *Journal of Geophysical Research: Oceans*, *125*, e2019JC015418. https://doi.org/10.1029/2019JC015418

Aouf, L., Dalphinet, A., Hauser, D., Delaye, L., Tison, C., Chapron, B., et al. (2019). On the assimilation of CFOSAT wave data in the wave model MFWAM: Verification phase. In *Proceedings of IGARSS 2019 – IEEE international geoscience and remote sensing symposium* (pp. 7959–7961). Yokohama. https://doi.org/10.1109/IGARSS.2019.8900180

Aouf, L., & Lefèvre, J.-M. (2015). On the impact of the assimilation of SARAL/Altika wave data in the operational wave model MFWAM. *Marine Geodesy*, *38*, 381–395. https://doi.org/10.1080/01490419.2014.1001050

Aouf, L., Lefèvre, J. M., & Hauser, D. (2006). Assimilation of directional wave spectra in the wave model WAM: An impact study from synthetic observations in preparation for the SWIMSAT Satellite mission. *Journal of Atmospheric and Oceanic Technology*, *23*, 448–463. https://doi.org/10.1175/JTECH1861.1

Ardhuin, F., Rogers, E., Babanin, A., Filippot, J.-F., Magne, R., Roland, A., et al. (2010). Semi empirical dissipation source functions for ocean waves. Part I: Definition, calibration, and validation. *Journal of Physical Oceanography*, *40*, 1917–1941. https://doi.org/10.1175/2010JPO4324.1

Babanin, A. V., Rogers, E. W., de Camargo, R., Doble, M., Durrant, T., Filchuk, K., et al. (2019). Waves and swells in high wind and extreme fetches, measurements in the Southern Ocean. *Frontiers in Marine Science*, *6*, 361. https://doi.org/10.3389/fmars.2019.00361

Badulin, S. I., Babanin, A. V., Zakharov, V. E., & Resio, D. (2007). Weakly turbulent laws of wind-wave growth. *Journal of Fluid Mechanics*, *591*, 339–378. https://doi.org/10.1017/S0022112007008282

Barbariol, F., Benetazzo, A., Bertotti, L., Cavaleri, L., Durrant, T., McComb, P., et al. (2019). Large waves and drifting buoys in the Southern Ocean. *Ocean Engineering*, *172*, 817–828. https://doi.org/10.1016/j.oceaneng.2018.12.011

Chapron, B., Johnsen, H., & Garello, R. (2001). Wave and wind retrieval from SAR images of the ocean. *Annales des Telecommunications*, *56*, 682–699. https://doi.org/10.1007/BF02995562

Collard, F., Ardhuin, F., & Chapron, B. (2005). Monitoring and analysis of ocean swell fields from space: New methods for routines observations. *Journal of Geophysical Research*, *114*, C07023. https://doi.org/10.1029/2008JC005215

Donelan, M. A., Hamilton, J., & Hui, W. H. (1985). Directional spectra of wind-generated waves. *Philosophical Transactions of the Royal Society of London*, *A315*, 509–562.

ECMWF. (2013). *Part VII : IFS documentation CY38R1, Part VII ECMWF wave model*. https://www.ecmwf.int/node/9248

Elfouhaily, T., Chapron, B., Katsaros, K., & Vandemark, C. D. (1997). A unified directional spectrum for long and short wind-driven waves. *Journal of Geophysical Research*, *102*, 15781–15796. https://doi.org/10.1029/97JC00467

Ewans, K. (1998). Observations of the directional wave spectrum of fetch-limited waves. *Journal of Physical Oceanography*, *28*, 498–512.

Fadaeiazar, E., Leontini, J., Onorato, M., Waseda, T., Alberello, A., & Toffoli, A. (2020). Fourier amplitude distribution and intermittency in mechanically generated surface gravity waves. *Physical Review E – Statistical Physics, Plasmas, Fluids, and Related Interdisciplinary Topics*, *102*, 013–106. https://doi.org/10.1103/PhysRevE.102.013106

Gerling, T. W. (1992). Partitioning sequences and arrays of directional ocean wave spectra into component wave systems. *Journal of Atmospheric and Oceanic Technology*, *9*, 444–458.

Gunther, H., Rosenthal, W., & Dunckel, M. (1981). The response of surface gravity waves to changing wind direction. *Journal of Physical Oceanography*, *11*, 718–728. https://doi.org/10.1175/1520-0485(1981)

Hasselmann, K., Barnett, P. T., Bouws, E., Carlson, H., Cartwright, E. D., Enke, K., et al. (01 1973). Measurements of wind-wave growth and swell decay during the Joint North Sea Wave Project (JONSWAP). *Deutsche Hydrographische Zeitschrift*, *8*, 1–95.

Hasselmann, K., Chapron, B., Aouf, L., Ardhuin, F., Collard, F., Engen, G., et al. (2012). *The ERS SAR Wave Mode – A breakthrough in global ocean wave observations*. (Vol.1326, pp. 167–197). European SpaceAgency, (Special Publication) ESA SP.

Hasselmann, D. E., Dunckel, M., & Ewing, J. A. (1980). Directional wave spectra observed during JONSWAP 1973. *Journal of Physical Oceanography*, *10*, 1264–1280.

Hasselmann, K., Ross, D. B., Muller, P., & Sell, W. (1976). A parametric wave prediction model. *Journal of Physical Oceanography*, *6*, 200–228. https://doi.org/10.1175/1520-0485(1976)006

Hauser, D., Tourain, C., Hermozo, L., Alraddawi, D., Aouf, L., Chapron, B., et al. (2020). New observations from the SWIM radar on-board CFOSAT: Instrument validation and ocean wave measurement assessment. *IEEE Transactions on Geoscience and Remote Sensing*, *59*, 1–22. https://doi.org/10.1109/TGRS.2020.2994372

Hsu, J. Y., Lien, R. C., D'Asaro, E. A., & Sanford, T. B. (2019). Scaling of drag coefficients under five tropical cyclones. *Geophysical Research Letters*, *46*, 3349–3358. https://doi.org/10.1029/2018GL081574

Kudryavtsev, V., Golubkin, P., & Chapron, B. (2015). A simplified wave enhancement criterion for moving extreme events. *Journal of Geophysical Research – C: Oceans*, *120*, 7538–7558. https://doi.org/10.1002/2015JC011284

Le Traon, P. Y., Reppucci, A., & Alvarez Fanjul, E. (2019). From observation to information and users: The Copernicus Marine Service Perspective. *Frontier in Marine Science*, *6*, 22. https://doi.org/10.3389/fmars.2019.00234

Lionello, P., Gunther, H., & Janssen, P. A. E. M. (1992). Assimilation of altimeter data in a global third generation wave model. *Journal of Geophysical Research*, *C97*, 14453–14474.

Long, C. E., & Resio, D. (2007). Wind wave spectral observations in Currituck Sound, North Carolina. *Journal of Geophysical Research*, *112*, CO5001. https://doi.org/10.1029/2006JC003835

Mitsuyasu, H., Tasai, F., Suhara, T., Mizuno, S., Ohkusu, M., Honda, T., et al. (1975). Observations of the directional spectrum of ocean waves using a clover leaf buoy. *Journal of Physical Oceanography*, *5*, 750–760.

Phillips, O. M. (1977). *The dynamics of the upper ocean* (2nd ed.). New York, NY: Cambridge University Press.

Pierson, W. J., & Moskowitz, L. (1964). A proposed spectral form for fully developed wind sea based on the similarity theory of S. A. Kitaigorodskii, J. *Journal of Geophysical Research*, *69*, 5181–5190. https://doi.org/10.1029/JZ069i024p05181

Schmale, J., Baccarini, A., Thurnherr, I., Henning, S., Efraim, A., Regayre, L., et al. (2019). Overview of the Antarctic circum navigation expedition: Study of preindustrial-like aerosols and their climate effects (ACE-SPACE). *Bulletin of the American Meteorological Society*, *100*, 2260–2283. https://doi.org/10.1175/BAMS-D-18-0187

Thurnherr, I., KozachekGraf, A. P., Weng, Y., Bolshiyanov, D., Landwehr, S., Pfahl, S., et al. (2020). Meridional and vertical variations of the water vapor isotopic composition in the marine boundary layer over the Atlantic and Southern Ocean. *Atmospheric Chemistry and Physics*, *20*, 5811–5835. https://doi.org/10.5194/acp-20-5811-2020

Toffoli, A., Onorato, M., Bitner-Gregersen, E. M., & Monbaliu, J. (2010). Development of a bimodal structure in ocean wave spectra. *Journal of Geophysical Research*, *115*, C03006. https://doi.org/10.1029/2009JC005495

Toffoli, A., Proment, D., Salman, H., Monbaliu, J., Frascoli, F., Dafilis, M., et al. (2017). Wind generated rogue waves in an annular wave flume. *Physical Review Letters*, *118*, 144503. https://doi.org/10.1103/PhysRevLett.118.144503

Vichi, M., Eayrs, C., Alberello, A., Bekker, A., Bennetts, L., Holland, D., et al. (2019). Effects of an explosive polar cyclone crossing the Antarctic marginal ice zone. *Geophysical Research Letters*, *46*, 5948–5958. https://doi.org/10.1029/2019GL082457

Young, I. R. (1999). Seasonal variability of the global ocean wind and wave climate. *International Journal of Climatology*, *19*, 931–950. https://doi.org/10.1002/(SICI)1097-0088(199907)19:9,931

Young, I. R., Fontaine, E., Liu, Q., & Babanin, A. V. (2020). The wave climate of the Southern Ocean. *Journal of Physical Oceanography*, *50*, 1417–1433. https://doi.org/10.1175/JPO-D-20-0031.1

Young, I. R., Verhagen, L. A., & Banner, M. L. (1995). A note on the bimodal directional spreading of fetch-limited wind waves. *Journal of Geophysical Research*, *100*(C1), 773–778.

Zieger, S., Babanin, A. V., Rogers, W. E., & Young, I. R. (2015). Observation-based source terms in the third-generation wave model WAVEWATCH. *Ocean Modelling*, *96*, 2–25. https://doi.org/10.1016/j.ocemod.2015.07.014